MICROBIOLOGY

Algicidal bacteria-derived membrane vesicles as shuttles mediating cross-kingdom interactions between bacteria and algae

Yixin Li[1]†, Yuezhou Wang[1]†, Xiaolan Lin[1]†, Shuqian Sun[1], Anan Wu[2], Yintong Ge[1], Menghui Yuan[1], Jianhua Wang[1], Xianming Deng[1]*, Yun Tian[1,3]*

Bacterial membrane vesicles (BMVs) are crucial biological vehicles for facilitating interspecies and interkingdom interactions. However, the extent and mechanisms of BMV involvement in bacterial-algal communication remain elusive. This study provides evidence of BMVs delivering cargos to targeted microalgae. Membrane vesicles (MVs) from *Chitinimonas prasina* LY03 demonstrated an algicidal profile similar to strain LY03. Further investigation revealed Tambjamine LY2, an effective algicidal compound, selectively packaged into LY03-MVs. Microscopic imaging demonstrated efficient delivery of Tambjamine LY2 to microalgae *Heterosigma akashiwo* and *Thalassiosira pseudonana* through membrane fusion. In addition, the study demonstrated the versatile cargo delivery capabilities of BMVs to algae, including the transfer of MV-carried nucleic acids into algal cells and the revival of growth in iron-depleted microalgae by MVs. Collectively, our findings reveal a previously unknown mechanism by which algicidal bacteria store hydrophobic algicidal compounds in MVs to trigger target microalgae death and highlight BMV potency in understanding and engineering bacterial-algae cross-talk.

INTRODUCTION

Most bacteria release membrane vesicles with diameters ranging from 20 to 400 nm that contain specific biologically active molecules and mediate multiple biological processes (*1*, *2*), including virulence (*3*), nutrition acquisition (*4*), bacterial competition (*5*), stress response (*6*), horizontal gene transfer (*5*, *7*), host survival (*8*, *9*), and cell-to-cell communication (*10*, *11*). The most remarkable property of these nanoparticles is that they can deliver a wide variety of bacterial products in high concentrations and in a protected manner to remote targeted cells (*12*). BMVs also have immunomodulatory activities, and all stages from biogenesis to transport are almost "engineerable" (*13*). Given that, BMVs not only are abundant in nature but are also great promising tools for vaccines (*14*), drug delivery vehicles (*15*), and for applications in synthetic biology and biotechnology. To date, our knowledge about BMVs and their role is mainly focused on model organisms in terms of cancerous-mammalian tissues (*16*, *17*), plant host–pathogen interactions (*18*), animal host-symbiont communications (*19*), and interbacterial competition (*5*, *20*). Many studies have demonstrated that BMVs can deliver multiple cargoes to their targeted cells (*21*) across the cell wall barrier of bacteria and plants to interact with their plasma membrane (PM), which could be achieved via a variety of ways, such as endocytosis (*22*, *23*), target cell membrane fusion (*20*, *22*, *24*), and insertion into the host PMs (*25*). These studies have made progress in our understanding of the functional role of BMVs and indicate that their shedding acts as a universal inter- and intrakingdom communication tool among all domains of life.

The bacteria-algal interaction is a typical representation of biological interkingdom communications and plays an important role in shaping the structure and function of ecosystems. Microalgae and bacteria can form complex, cross-kingdom units in various natural environments, and the exchange of metabolites and infochemicals governs bacteria-algal relationships, which span mutualism, commensalism, antagonism, parasitism, and competition (*26*). As nutrient complementarity is fundamental for the stability of bacteria-algal units, multiple lines of evidence have verified that bacteria can release a wide range of metabolites, such as vitamin B_{12}, indole-3-acetic acid, and siderophores, to the phycosphere, which are subsequently consumed by algae (*27*–*31*), along with the discovery of membrane transporters involved in the acquisition of these key nutrients in algae (*32*). In addition, acting as intra- and interkingdom languages used by microorganisms, bioinfochemicals are proven to shape the modes of bacteria-algal interaction (*33*), such as acyl homoserine lactones (*34*), 2-heptyl-4-quinolone (*35*), deinoxanthin (*36*), and prodigiosin (*37*). Certain bioactive molecules can even be fatal to algae, triggering algae lysis, driving the algae-killing process and thus playing a very important role in the control of harmful algal blooms (HABs) (*38*). The importance of bacteria-algal interactions has been postulated for four decades, but our understanding of the complex nature of this unique microbial theater is still limited by technical and conceptual limitations. Although the horizontal shuttle functions of BMVs for inter- and intrakingdom communication are evident, it is totally unknown whether and how BMVs are involved in the cross-talk between bacteria and algae as cargo carriers by recognizing certain channels in microalgae. Therefore, physiologically relevant evidence for the transfer of functional biomolecules from bacteria to individual algae cells by BMVs is urgently needed.

[1]State Key Laboratory of Cellular Stress Biology, School of Life Sciences, Xiamen University, Xiamen 361102, China. [2]State Key Laboratory for Physical Chemistry of Solid Surface, College of Chemistry and Chemical Engineering, Xiamen University, Xiamen, China. [3]Key Laboratory of the Ministry of Education for Coastal and Wetland Ecosystems, Xiamen University, Xiamen 361102, China.
*Corresponding author. Email: tianyun@xmu.edu.cn (Y.T.); xmdeng@xmu.edu.cn (X.D.)
†These authors contributed equally to this work.

In our previous study, a high-efficiency algicidal bacterium, *Chitinimonas prasina* LY03, was isolated and found to produce yellow-green pigment at the stationary phase (*39*). Detection of the algicidal activity of LY03 cells and cell-free supernatants was conducted, and scanning electron microscopy (SEM) images of the coculture with HAB-causing algae *Thalassiosira pseudonana* showed that algal cells adhered by strain LY03 were lysed with severely damaged cellular structure, suggesting that LY03 may induce algal death by like cell-cell contact (*40*). However, which compounds are involved in the algicidal process and how they interact with microalgae are still obscure. In the present study, a large number of MVs released from LY03 (LY03-MVs) were first observed. The purified MVs were then applied for the determination of algicidal activity and spectrum to confirm the involvement of LY03-MVs in the algicidal process. Wild-type and mutant strains were subjected to comparative genomic, transcriptomic analysis and algicidal compound mapping to reveal the loading and delivery of yellow-green pigments via LY03-MVs to kill targeted microalgae. Direct evidence for membrane fusion between LY03-MVs and microalgae was then captured and visualized by using fluorescent dyes and imaging techniques. Furthermore, in combination with tracking experiments and physiological tests, we found that MVs could also deliver genetic materials and iron to microalgae. The results of our study provide the direct evidence of the horizontal transfer of functional biomaterials from bacteria to individual microalgae cells via BMVs, which not only reveals a previously unknown algicidal mechanism mediated by BMVs but also opens a window that allows us to obtain distinctive insight to understand, characterize, and even manipulate bacteria-algae interactions.

RESULTS

Membrane vesicles from *Chitinimonas prasina* LY03 mediate targeted killing of microalgae

To characterize the membrane vesicles released by LY03, the morphology of LY03 in the stationary phase was observed using transmission electron microscopy (TEM) and SEM. Both TEM and SEM observed MVs, when TEM showed that a considerable number of MVs were secreted via membrane blebbing from LY03, and most of them adhered to the cell surface (Fig. 1A, left). The crude extract of LY03-MVs were then obtained and showed highly efficient algicidal activity against the harmful bloom-forming alga *Heterosigma akashiwo* in a concentration-dependent manner (Fig. 1A, right). The MVs were further purified using density gradient centrifugation and were mainly detected in fractions 4 to 6, with fraction 5 showing the highest concentration of MVs (Fig. 1B). The purification allowed TEM to image MVs clearly as distinct saucer-shaped structures (a few tube-shaped structures), which consist of two bilayer membranes derived from the outer membrane and the inner membrane, with sizes ranging from 47 to 168 nm as measured by nano–flow cytometry (Nano FCM) for all MVs (Fig. 1C). Meanwhile, the purified MVs from fraction 5 also displayed the highest algicidal activity with the same algicidal spectrum as the cells of LY03 (Fig. 1D), indicating that LY03-MVs could mediate targeted killing of microalgae. The purified LY03-MVs were further treated with proteinase K and nuclease, resulting in no substantial change in algicidal activity against *H. akashiwo* (fig. S1), suggesting that the algicidal active substance likely be a small molecular compound harbored and protected in LY03-MVs. In addition, we found that BMVs are stable in sterile seawater, as their size and concentration remained essentially unchanged, and they maintained high algicidal activity over the course of 10 days, inferring that LY03-MVs might maintain robust algicidal activity in natural environments for a long period of time (Fig. 1, E and F). These results strongly indicated that LY03-MVs can carry algicidal compounds and deliver them to targeted microalgae, which eventually lead to algal mortality.

Production of yellow-green pigment is responsible for the algicidal activity of LY03

In our previous study, LY03 was found to produce yellow-green pigment and exhibit algicidal activity at the stationary phase (*39*). During the cultivation of LY03, a spontaneous mutant strain without yellow-green pigment production was obtained and named QY03 (Fig. 2A, left). Compared with LY03, the pigment-null strain QY03 lost algicidal activity (Fig. 2A, right), indicating that yellow-green pigment production may be responsible for algicidal activity. To verify this hypothesis and identify the involved genes, the transcriptomes of LY03 and QY03 were comparatively analyzed (Fig. 2B). In total, 2313 and 2316 genes were up-regulated significantly in LY03 at the stationary phase (LY03-S) in comparison to that in LY03 at the exponential phase and that in QY03 at the stationary phase (QY03-E). Among the up-regulated genes with highest fold changes (fig. S2, A and B), 14 of 20 genes were related to pigment biosynthesis, some of which were found to be involved in the biosynthesis of prodiginine (*41*) (a red triliprolic bacterial pigment) and tambjamine (*42*) (a yellow biprolic bacterial pigment). Moreover, these 14 genes were predicted to constitute a gene cluster, with other 7 adjacent genes, which were also significantly up-regulated (fig. S2C), indicating that these 21 clustered genes (named as *TalA*-*TalU*) are responsible for yellow-green pigment biosynthesis (Fig. 2C and table S1). Furthermore, whole-genome resequencing was also applied to QY03, and 21 mutation sites were detected, therein a nonsense mutation in *TalU* encoding transcriptional activator protein was found, supporting the prediction of the pigment biosynthetic gene cluster (Fig. 2C and fig. S3). A key gene for pigment synthesis was then selected and deleted to generate mutant Δ*TalD*, and the algicidal activity assays showed that the purified MVs of Δ*TalD* (Δ*TalD*-MVs) and QY03 (QY03-MVs) exhibited no algicidal activity, whereas the LY03-MVs showed high-efficiency algicidal activity ($P < 0.0001$) (Fig. 2D), indicating that LY03-MVs may carry yellow-green pigment to kill targeted microalgae.

Tambjamine LY2 is the algicidal compound loaded by MVs

To identify the algicidal compound(s) produced by LY03, we compared the metabolic profiles of LY03, QY03, and mutant Δ*TalD*. Unique peaks in LY03 identified using liquid chromatography–mass spectrometry (LC-MS) analysis are expected to correspond to the peaks of algicidal compounds. Two unique peaks, 1 and 2, with mass/charge values of 442.2 and 382.3, respectively, were specifically found in the organic extract of the total culture of LY03 (Fig. 3A), which were further purified and tested for algicidal activity. Compound **2** showed a dose-dependent killing effect on *H. akashiwo* with an median inhibitory concentration (IC_{50}) value of 2.377 μM, while compound **1** barely showed any algicidal activity (Fig. 3, B and C), suggesting that compound **2** is the major algicidal compound produced by LY03.

Analysis of one-dimensional (1D) (^{1}H and ^{13}C) and 2D [correlation spectroscopy (COSY), heteronuclear single-quantum coherence (HSQC), and heteronuclear multiple-bond correlation (HMBC)]

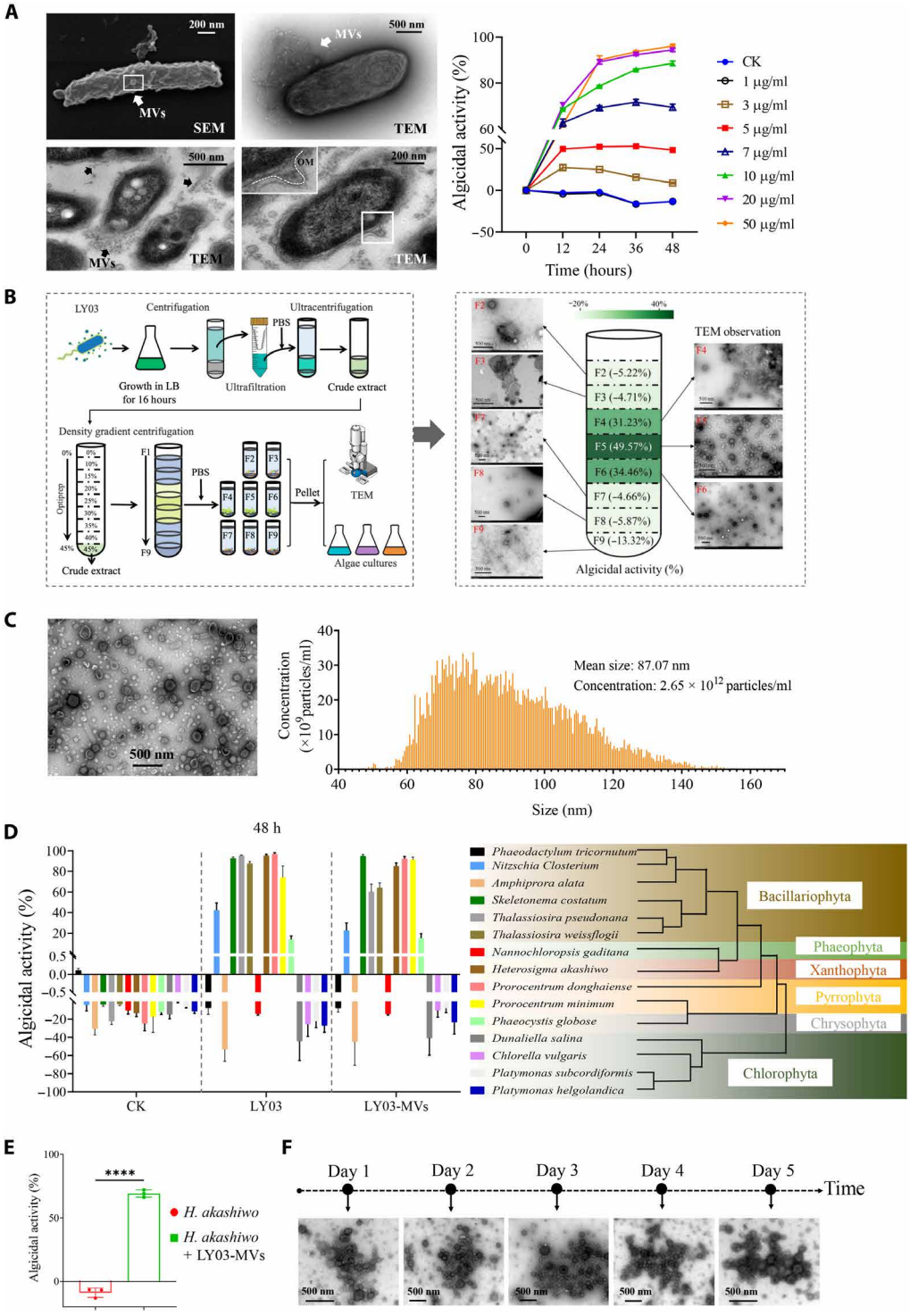

Fig. 1. Observation, purification, and characterization of membrane vesicles generated by LY03. (**A**) Representative TEM and SEM images of LY03 cells with MV blebbing (left) and the algicidal activity determination of different concentrations of the crude LY03-MVs (right). OM indicates outer membrane. (**B**) The flow chart of MV purification and the algicidal activity and TEM images of each density gradient ultracentrifugation fraction. (**C**) Particle size and concentration analysis using Nano FCM and TEM imaging of purified LY03-MVs. (**D**) The algicidal spectrum of LY03 and LY03-MVs. (**E**) The algicidal activity of LY03-MVs after being stored in f/2 medium for 10 days against *H. akashiwo*. Asterisks indicate statistically significant (****$P < 0.0001$) differences. (**F**) Negative-staining micrograph of LY03-MVs stored in f/2 medium for 1 to 5 days.

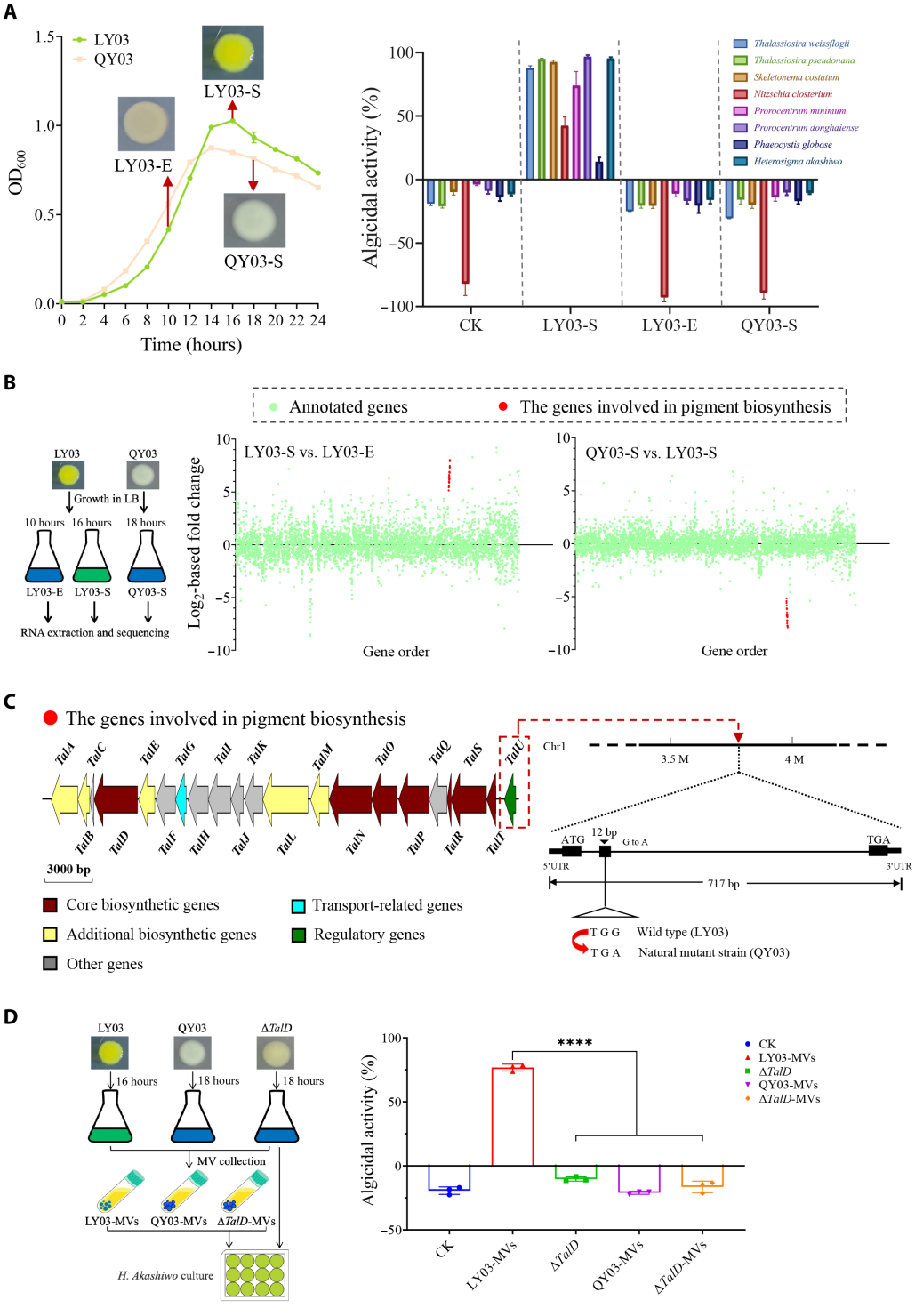

Fig. 2. Analysis of the relationship between algicidal activity and production of yellow-green pigments by LY03 and identification of genes involved in pigment biosynthesis. (**A**) The growth curve, colony morphology (left), and algicidal spectrum (right) of LY03 and its pigment-null mutant strain QY03 at the stationary phase (-S) and exponential phase (-E), respectively. (**B**) Gene differential expression analysis of the transcriptome of LY03 at the stationary phase against that of LY03 at the exponential phase and that of QY03 at the stationary phase. The relative gene transcriptional levels were transcribed as $\log_2$ fold change. Each dot represents a gene, with each gene distributed on the *x* axis in accordance with the locus tag number for LY03. Genes more highly transcribed are present above the *x* axis, and those transcribed at a lower level are present below the *x* axis. S and E indicate the stationary phase and exponential phase, respectively. (**C**) The putative pigment biosynthetic gene cluster and the mutation site analysis of *TalU*. 5′UTR, 5′ untranslated region. (**D**) The algicidal activity of mutant Δ*TalD* and MVs produced by LY03, QY03, and Δ*TalD*. Asterisks indicate statistically significant (****$P < 0.0001$) differences.

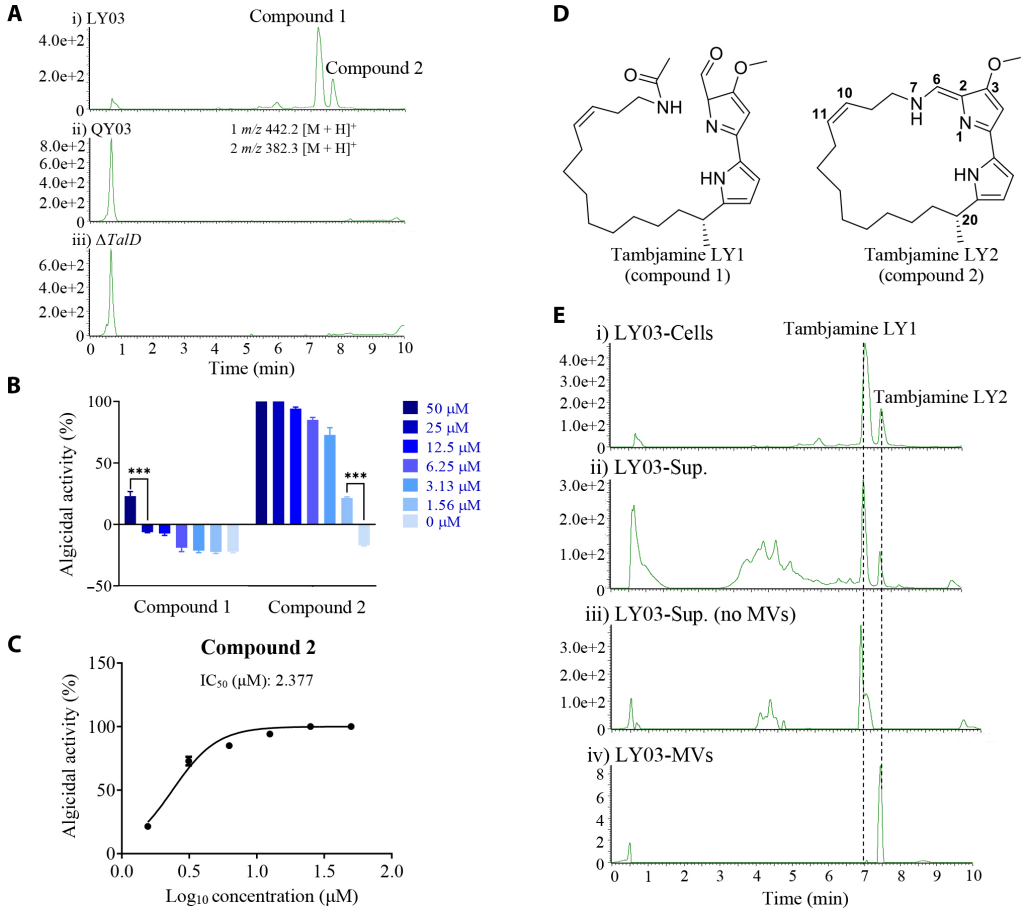

Fig. 3. Identification and positioning of algicidal compounds. (**A**) LC-MS analysis of total culture extracts of strains LY03, QY03, and mutant Δ*TalD*. *m/z*, mass/charge ratio. (**B**) Algicidal activity of compounds **1** and **2**. Asterisks indicate statistically significant (***$P < 0.001$) differences. (**C**) IC_{50} value of compound **2**. (**D**) Chemical structure of Tambjamine LY1 (compound **1**) and Tambjamine LY2 (compound **2**). (**E**) LC-MS analysis of organic extracts of different culture components of LY03. i) Bacterial cells (LY03 cells), ii) cell-free supernatants (LY03-Sup.), iii) MV-free supernatant [LY03-Sup. (no MVs)], and iv) purified MVs (LY03-MVs).

nuclear magnetic resonance (NMR) spectra and high resolution mass spectrometry (HR-MS) data revealed that compounds **1** and **2** are two unreported tambjamine family antibiotics that contain a conserved bipyrrole core functionalized with alkylimines. By comparing the spectral data of compounds **1** and **2** and the corresponding literature tambjamine MYP1 (*42*), we found that compounds **2** and MYP1 are both macrocyclized tambjamines. The key difference between compounds **2** and MYP1 is the presence of an additional methylated methine in compound **2**. Compound **1** is a linear tambjamine with acetylated alkylamine and bipyrrole-carboxaldehyde moieties (Fig. 3D). The absolute configurations of compounds **1** and **2** were established according to nuclear Overhauser effect spectroscopy analysis, *J*-couple analysis, and quantum chemical calculations (Supplementary Text), and compounds **1** and **2** were named Tambjamine LY1 and Tambjamine LY2, respectively.

To examine whether the LY03-MVs potentially serve as delivery vehicles for Tambjamine LY1 and/or Tambjamine LY2, we cultured LY03 to stationary phase (LY03-S) and collected samples from the culture (LY03 Cells), cell-free supernatant (LY03-Sup.), supernatant after the removal of MVs [LY03-Sup. (no MVs)], and MVs from the supernatant (LY03-MVs). LC-MS analysis showed that Tambjamine LY2 was detectable in all MV-containing samples (LY03-Cells, LY03-Sup., and LY03-MVs) but not in the MV-free supernatant sample [LY03-Sup. (no MVs)], whereas Tambjamine LY1 was absent in LY03-MVs but detectable in all the other samples, including LY03-Cells, LY03-Sup., and LY03-Sup. (no MVs) (Fig. 3E), indicating that Tambjamine LY2 was selectively packaged into LY03-MVs and can be secreted extracellularly by loading in MVs.

LY03-MVs deliver Tambjamine LY2 to the targeted microalgae via membrane fusion

To explore how LY03 cells and MVs contact and react with algal cells when they cocultured, enhanced green fluorescent protein (eGFP)–labeled LY03 cell (eGFP-LY03) was constructed first to make it traceable, and then its response to FM4-64–labeled microalgae *H. akashiwo* and *T. pseudonana* was monitored using automated live cell imaging systems (Fig. 4A and movies S1 and S2). The images illustrated that eGFP-LY03 appeared capable of consecutively turning toward the motile algae, recovering from the occasional wrong turn and continuing to move and accumulate around the swimming algae, indicating that LY03 can be attracted by moving algae and form transient phyto-bacterial associations. Meanwhile, the chemotactic response of LY03 to *T. pseudonana* and *H. akashiwo* was evaluated by quantitative capillary and titration plate assays. As shown in fig.

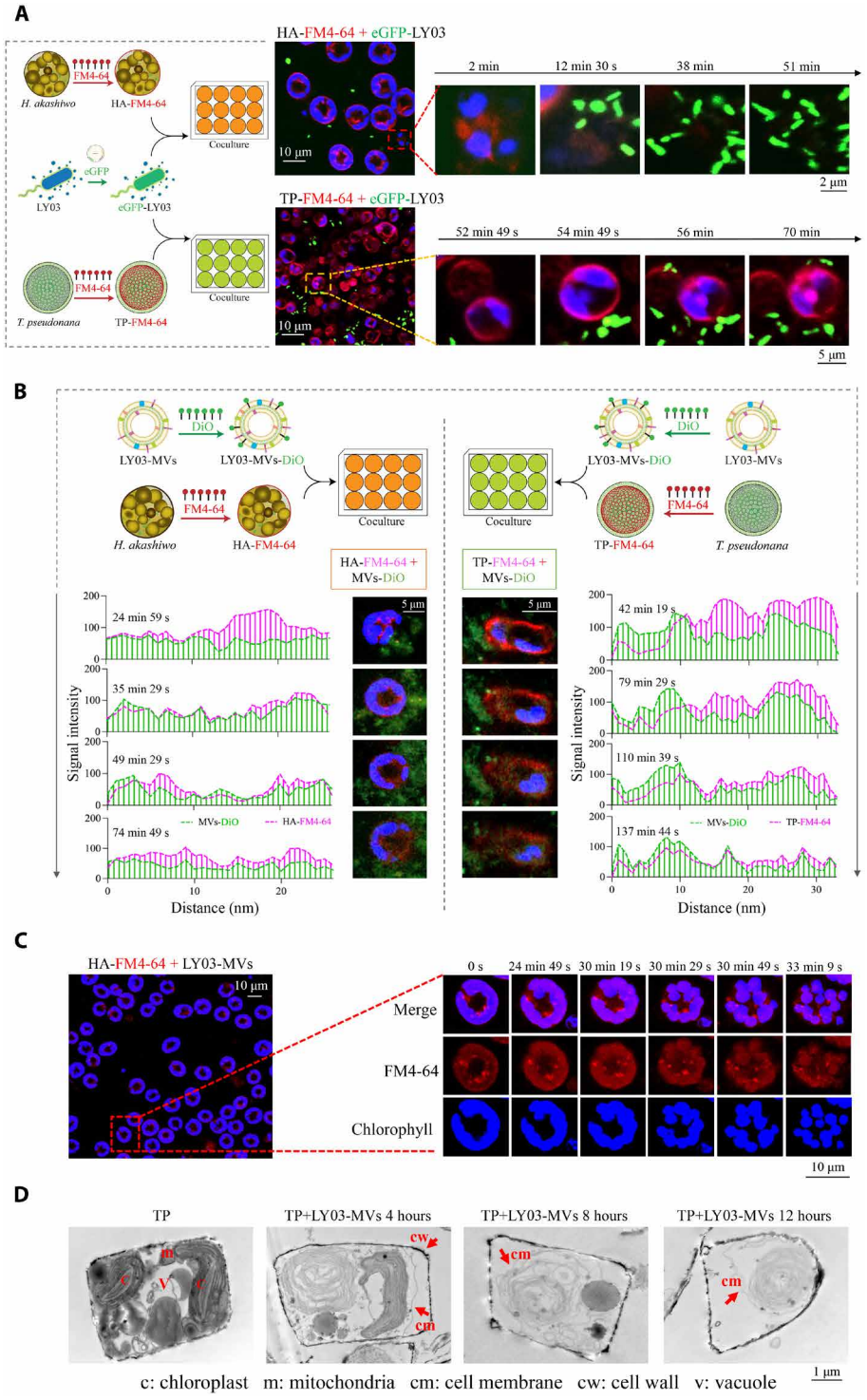

Fig. 4. Visualization of interactions between LY03, LY03-MVs, and the targeted microalgae. (**A**) Images captured from the video observation of bacterial chemotaxis of LY03 toward algae *H. akashiwo* and *T. pseudonana*. Algal cell membranes were labeled by the styryl fluorescent membrane marker FM4-64 (red). (**B**) Visualization of interactions between LY03-MVs and algae *H. akashiwo* and *T. pseudonana* after incubation for 3 hours by fluorescence microscopy. MVs were stained with the lipophilic dye DiO (green), and microalgal cell membranes were labeled with FM4-64. The spontaneous fluorescence of chloroplasts in algae showed blue signals. Fluorescence colocalization analysis of the resulting images was performed using FIJI software. The morphological changes in *H. akashiwo* (**C**) and *T. pseudonana* (**D**) under LY03-MV treatment were observed by using automated live-cell imaging systems and TEM, respectively. HA and TP in the above figures indicate *H. akashiwo* and *T. pseudonana*, respectively.

S4, strain LY03 showed chemotactic activity toward algae, demonstrating that the aforementioned observations are chemotactic responses of LY03 to the target algal cells.

LY03-MVs obtained at stationary phase were stained with the lipophilic dye DiO and incubated with FM4-64–labeled microalgae (*T. pseudonana* and *H. akashiwo*), and then their interaction was visualized (Fig. 4B and movies S3 and S4). As shown in Fig. 4B, large amounts of LY03-MVs attached to the surface of microalgae, and their interactions were supported by their colocalization according to their similar curve patterns of fluorescent signal intensity. The morphological observation of FM4-64–labeled *H. akashiwo* under LY03-MV treatment showed a serious disruption in the cell membranes (Fig. 4C and movie S5). At the same, the flow cytometry assay displayed a significantly increased number of PI-stained cells (P1 area), which represent *H. akashiwo* with high membrane permeability (fig. S5), suggesting that their cell membranes were damaged by LY03-MVs. With regard to *T. pseudonana*, the TEM images revealed alterations in ultrastructure under the algicidal effects of LY03-MVs (Fig. 4D). As the algal cells in the control samples exhibited normal cellular morphology with compact cell structure and intact organelles arranged in an orderly pattern, the morphology and structure of the cell membrane and organelles were seriously damaged, with the siliceous shell remaining intact for those cells under LY03-MV treatment. Together, these results indicated that pigment-loaded MVs could across the cell wall barrier to interact with and destroy algal cell membranes.

To determine how MVs interacted with the target microalgal membrane, LY03-MVs were labeled with octadecyl rhodamine B chloride (R18), which does not fluoresce individually, followed by incubation with microalgae, and fluorescence can be triggered when R18-labeled MVs fused with algal cell membranes (Fig. 5A). MVs and three targeted algal cells (*T. pseudonana*, *H. akashiwo*, and a reference species, *Phaeodactylum tricornutum*, which is resistant to LY03 and LY03-MVs) were also stained with R18 separately, and the absence of fluorescence at 0 hours (fig. S6) and 2 hours [R18 only groups in Fig. 5 (B and C)] ruled out the possibility of unexpected fluorescence emitted by R18-labeled MVs and algal cells themselves. Then, the R18-labeled MVs were incubated with three targeted microalgae, and after a 2-hour incubation, there were noticeable increases in fluorescence signals located in the cell membranes of LY03-sensitive microalgae *H. akashiwo* and *T. pseudonana* regardless of whether they were treated with pigment-loaded or pigment-deficient LY03-MVs obtained at stationary and exponential phases (LY03-S-MVs and LY03-E-MVs), respectively (Fig. 5, B and C), but no fluorescent signals were detected for LY03-resistant algae *P. tricornutum*, indicating that LY03-MVs interacted with algal cells via membrane fusion species specifically and that their membrane fusion ability was unrelated to the presence of pigment. Thus, multiple pieces of evidence confirm that LY03-MVs interacted with targeted microalgae via membrane fusion, which facilitate the transport of algicidal compound Tambjamine LY2 into algal cells and trigger the algae-killing process.

LY03-MVs deliver cargos other than algicidal pigment to microalgae

To explore whether BMVs are capable of delivering other functional cargoes, we characterized their protein and metabolite contents using LC–tandem MS (LC-MS/MS), resulting in 1047 proteins and 446 metabolites were detected. The majority of proteins were located at cytoplasm and cytoplasmic membrane (58.6%), when the others were outer membrane, periplasmic, and extracellular proteins (fig. S7A). As shown in fig. S7B, 889 proteins were classified into 19 clusters of orthologous genes (COG) functional categories. The proteins related to amino acid transport and metabolism and cell wall/membrane biogenesis were predominant, followed by energy production and conversion, inorganic ion transport and metabolism, and signal transduction. Regarding to metabolites of MVs, they were mainly classified into 18 categories, with dominance of those affiliated to metabolism of secondary metabolites and amino acid and membrane transport (fig. S8).

Among 25 proteins classified into nucleotide transport and metabolism, most of them were involved in nucleotide biosynthesis, so we first tested whether LY03- and Δ*TalD*-MVs can package genomic DNA and exogenous plasmids. Polymerase chain reaction (PCR) experiments detected targeted genes (table S2) in LY03- and Δ*TalD*-MVs generated at the stationary phase (fig. S9), demonstrating that DNA was packed into MVs. Further confocal microscopic inspection of both 4′,6-diamidino-2-phenylindole (DAPI)–stained Δ*TalD*-MVs incubated with LY03-sensitive *T. pseudonana* and LY03-resistant *P. tricornutum* and DAPI-stained LY03-S-MVs incubated with *P. tricornutum* revealed the presence of MV-derived DNA intracellularly in *P. tricornutum* and *T. pseudonana* (Fig. 6A). These results provide evidence for MV-mediated DNA delivery to microalgae.

Given the dominance of proteins involved in ion transport in MVs and the crucial role of BMVs in iron acquisition in a wide variety of bacterial species (*43*), the potential of LY03-MVs in iron delivery was examined. The coincubation systems of LY03-sensitive *H. akashiwo* and *T. pseudonana* with LY03-E-MVs and LY03-resistant *P. tricornutum* with LY03-E- and LY03-S-MVs were constructed. The groups treated with iron-incubated MVs were also set up. As shown in Fig. 6B, compared with the control samples, the addition of LY03-S-MVs and iron-incubated MVs significantly promoted the growth of the iron-depleted algal cultures, when the iron-incubated MV treated samples showed the highest growth rate, indicating that MVs can take up surrounding iron and mediate interkingdom iron delivery. Moreover, the algal cultures adding EDTA-treated iron-incubated MVs were also monitored, resulting in similar growth rates comparing to the groups without EDTA treatment, suggesting that the iron was encapsulated inside the MVs rather than surface-attached. Further assay tested the occurrence of siderophores, and the result showed the absence of siderophores neither in LY03 cells nor LY03-MVs (fig. S10), inferring that siderophore was unlikely the mediator for iron acquisition of LY03. Overall, these data strongly implicated that BMVs can shuttle varied cargoes across cell wall barriers to microalgae in multiple ways.

DISCUSSION

Released by virtually all living organisms, MVs are now regarded as a vital mode of inter- and intrakingdom communication (*44*, *45*). Here, we present an underestimated role of MVs in bacteria-algae cross-talk from the view of BMV-mediated algae killing. Against the background of increasing algal blooms, algicidal bacteria inhabiting the phycosphere exhibit complex interactions with algae and decisive effects on the decline in algal blooms (*46*), so there is a growing awareness of exploring the underlying mechanisms for their application in harmful algae control. To date, alginolysis is known to be

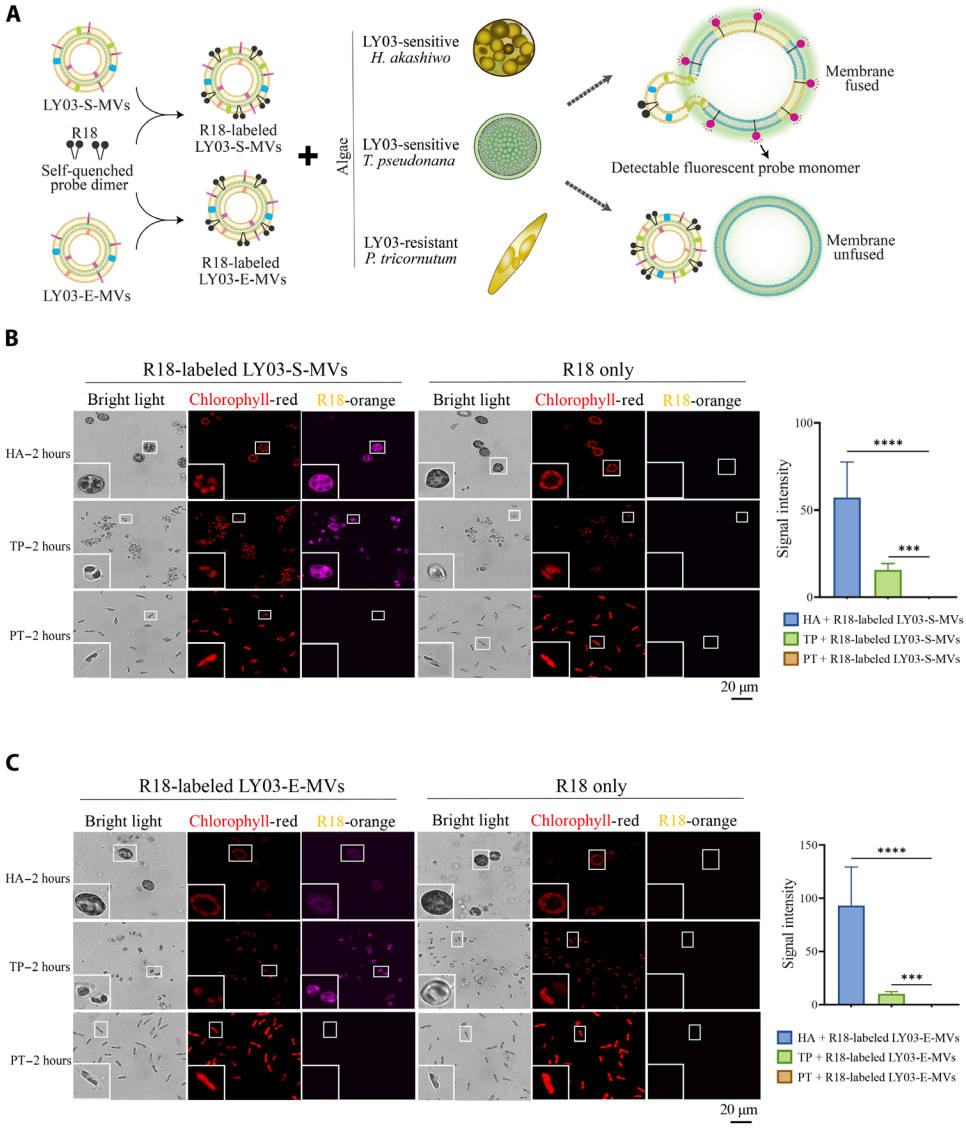

Fig. 5. Visualization of membrane fusion between MVs with the targeted algae by confocal microscopy. (**A**) The schematic diagram of membrane fusion test experiments. The confocal tracking of algal cells after incubating with and without R18-labeled LY03-S-MVs (**B**) and LY03-E-MVs (**C**) for 2 hours. Algal cells and MVs were stained with R18 by incubation for 1 hour. The three targeted microalgae were *H. akashiwo* (HA), *T. pseudonana* (TP), and *P. tricornutum* (PT). Asterisks indicate statistically significant (***$P < 0.001$ and ****$P < 0.0001$) differences.

executed by bacterial algicides in direct and indirect patterns, which are achieved through direct cell-to-cell interactions and release to the extracellular milieu, respectively (*47*). However, in this study, we found that BMV secretion was required for algae killing. A potent algicidal compound named Tambjamine LY2 was identified with significant hydrophobic character and proved to be selectively packaged into MVs. The following tracking experiments further confirmed that these algicide-embodied MVs could be delivered to and interacted with algae cells via membrane fusion, ultimately leading to algae lysis. These findings indicated a targeted algae-killing mode through the horizontal transmission of hydrophobic algicidal compounds by MV shuttling, expanding our understanding of bacteria-algae interactions from a previously unknown perspective.

In comparison to two classic modes whose underlying mechanisms have not yet been elucidated, the BMV-mediated algicidal mode shows substantial advantages. On the one hand, compared to the contact-dependent algicidal mode (*48*), BMVs can be considered reflective of their producing cells, and the BMV-mediated algicidal process allows parental bacteria to release a large number of their substitutes and transport concentrated boluses of algicidal compounds to targeted cells, contributing to a more specific attack range and broader contact area without the need for direct cell-to-cell contact. On the other hand, considerable amounts of algicidal bacteria kill algae cells by releasing algicides into the extracellular milieu (*36*, *37*). However, a problem arises is that these algicidal compounds are usually hydrophobic and diffuse randomly in an aqueous environment (*47*), resulting in diluted concentrations and significantly decreased algicidal efficiency in practice. The lipidic nature makes BMVs highly suitable for delivering hydrophobic molecules (*20*, *22*, *49*), which enables BMVs to embed hydrophobic algicidal

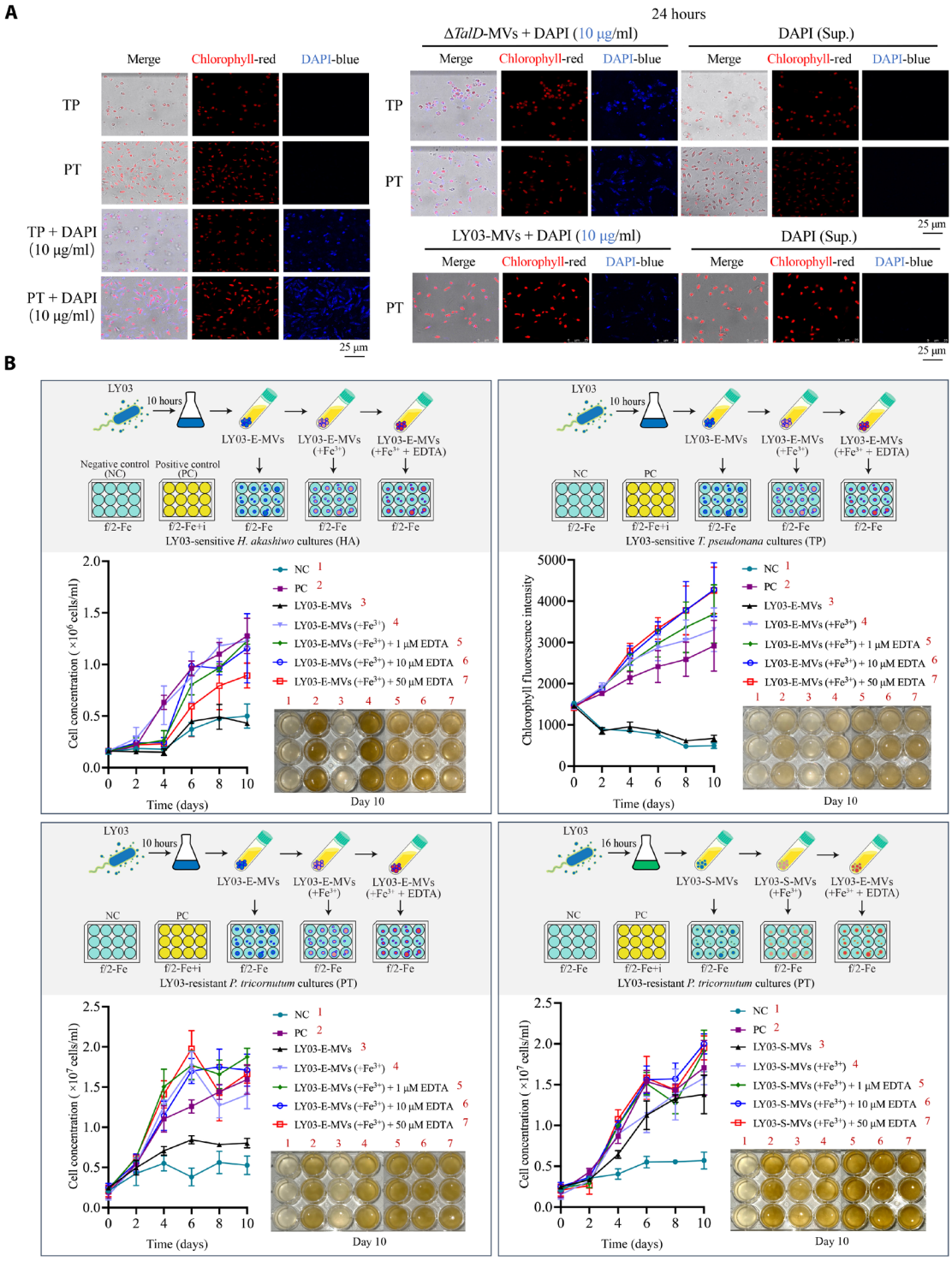

Fig. 6. Detection of MV-mediated DNA and iron delivery to microalgae. (**A**) The colocalization of MV-associated DNA with targeted microalgae based on confocal microscopy. The left showed the targeted microalgae labeled with and without DAPI (10 μg/ml) that regarded as the positive and negative controls. The right displayed the incubation of targeted microalgae with DAPI-stained MVs (LY03- and Δ*TalD*-MVs) and the supernatant after MV collection (Sup.) for 24 hours at 25°C, respectively. The two targeted microalgae were *T. pseudonana* (TP) and *P. tricornutum* (PT). (**B**) The coculture experiment of algae and LY03-MVs under iron-deficient conditions. LY03-MVs, iron-incubated LY03-MVs, and EDTA-treated iron-incubated LY03-MVs added to algal cultures grown in iron-deficient f/2 medium (f/2-Fe) as the sole iron source, respectively. NC indicates a negative control for HA, TP, and PT cultivated in f/2-Fe medium, and PC indicates a positive control for HA, TP, and PT cultivated in f/2-Fe medium with ferric iron addition (f/2-Fe + i). HA, TP, and PT represent *H. akashiwo*, *T. pseudonana*, and *P. tricornutum*, respectively.

compounds at high loading and protect them from enzymatic degradation before reaching targeted distant cells (*50*). Our results also proved that BMVs are stable in seawater, highlighting the sustainability of the protective ability of BMVs. Furthermore, both classic algicidal modes generally have low species specificity, which may lead to a decline in harmless algae and even ecosystem imbalance (*47*). The oriented delivery and membrane fusion of BMVs to algae cells provides the possibility that some moieties can be equipped or modified on the surface of BMVs by surface engineering (*51*) to enhance or alter the targeted delivery of diverse algicidal compounds to specific microalgae while preserving the integrity of the vesicles. Thus, by acting as shuttles of algicides between bacteria and algae, BMVs are expected to be a promising tool as an algicidal nanomaterial to control harmful algae blooms with high efficiency and specificity.

In addition to the potential in the application of harmful algae control, the ability of BMVs to encapsulate a variety of bioactive molecules and achieve directional delivery to algae cells may offer a window into the characterization and even manipulation of cross-kingdom communication. BMVs have been reported to incorporate vitamin K2 and fatty acids and be beneficial to host health (*52*). In contrast, BMVs produced by many pathogenic bacteria play essential roles in delivering various virulence-related molecules, such as quorum sensing signals, proteases, and hydrolases, which are able to kill host cells (*53*). In our study, in addition to the algae-lysing pigment, iron was also verified as one of the cargoes delivered by LY03-MVs. Iron is an indispensable nutrient for microbes but is difficult to acquire. There is increasing evidence pointing toward the presence of iron as one of the main cargos in BMVs and an important role of BMVs in iron acquisition (*54*). Wang *et al.* (*43*) reported that MVs released by the Gram-positive bacterium *Dietzia* sp. DQ12-45-1b acts as a pathway for extracellular heme recycling from hemoproteins in surrounding environments. They also proved that heme-carrying MVs can act as a public good shared between phylogenetically closely related species, making a great contribution to their enhanced iron acquisition ability. In comparison to bacteria, unicellular photosynthetic species exhibit higher iron demands, and iron availability is considered a vital limiting factor for the growth of primary producers such as diatoms (*55*). Some studies have demonstrated that bacteria can facilitate the growth of algae under iron-deficient conditions by enhancing the availability of iron or providing siderophores (*56*). In the present study, we proved that MVs derived from LY03 could capture iron and significantly facilitate the growth of the LY03-resistant diatom *P. tricornutum* under iron-deficient conditions, strongly suggesting the capability of BMVs to deliver iron into microalgal cells, acting as public goods in bacteria-microalgae interkingdom communication. In addition, LY03-MVs generated at the exponential phase can also promote the growth of iron-deficient *T. pseudonana*, which can be lysed by stationary phase LY03-MVs, showing the functional role transition of MVs from killers to helpers, which likely leads to a change in the bacteria-microalgae crosstalk channels and their interactional modes. This finding provided dynamic scenarios of bacteria-microalgae interactions across the different stages of an algal bloom and an uncovered but essential role of MVs in this marked relationship shift via delivery of different cargoes, extending our understanding of the complex interactions between microalgae and bacteria. Together, our results demonstrated the conditional cargo loading capability of MVs and their diverse functional cargos, and these characteristics raise a possibility of modulating bacteria-microalgae interactions and even oriented functional enhancement, accomplished by altering cargoes in a targeted manner.

Detectable plasmid DNA and partial genomic DNA were packaged in BMVs, indicating that DNA was another cargo of BMVs. The incubation of DAPI-stained MVs with *T. pseudonana* and *P. tricornutum* further confirmed the presence of MV-encapsulated DNA in targeted microalgae, suggesting that BMVs can penetrate through the algae barriers and deliver DNA to microalgal cells. These findings suggest that BMVs could be used as DNA carriers to achieve horizontal gene transfer between bacteria and algae. As diatoms are the largest group of biomass producers on Earth (*57*), *T. pseudonana* is model diatom that shows significance in algal biotechnology and fuel production (*58*) and has been studied with meta-omics approaches as well as a few genetic tools (*59*). However, the efficiency of these available genetic tools was unsatisfactory for *T. pseudonana* due to its silicified cell walls (frustules), limiting further application. Taking advantage of their span and DNA-carrying capability, BMVs may be a highly promising rookie for diatom genetic engineering.

Another thing worth mentioning is that although membrane fusion was not observed between MVs and *P. tricornutum*, MV system was verified to deliver iron and DNA to *P. tricornutum*, inferring a possibility of other mechanism that enable MV to associate with and deliver cargos to algal cells. To our knowledge, there are five pathways for MV uptake, including membrane fusion and four types of endocytosis (macropinocytosis, clathrin-mediated endocytosis, caveolin-mediated endocytosis, and lipid raft–mediated endocytosis), which are mainly focus on bacteria, mammals, and plants (*53*, *60*, *61*). But given that the interaction between BMVs and microalgae was rarely reported, there is a scarcity of relevant studies offering insights or adequate methodologies to clearly elucidate the mechanisms underpinning the uptake process, and further more studies are needed to establish robust and efficient approaches to better address this question.

In summary, our study found out a potentially manipulative interkingdom communication system between bacteria and algae mediated by BMVs (Fig. 7). On the basis of the discovery of the involvement of BMVs in algae killing, captured direct evidence demonstrated that BMVs can function as shuttles encapsulating and delivering multiple cargos, including algicidal pigments, iron, and DNA, to targeted algae cells. Our findings characterized BMVs as a powerful means of bacteria-algae cross-talk on account of their selectivity for effective algicides, long-term protective capability for cargoes, targeted delivery manner, and ability to penetrate through algae barriers. These features allow the BMV system to be a promising tool for better exploring and even modulating bacteria-algae interactions, exhibiting significance in further applications of harmful algae control and microalgae genetic engineering.

METHODS

Bacterial strains, algae, and culture conditions

A detailed bacterial strain list used in this study can be found in table S2. LY03 and relevant mutants were grown in nutrient agar (NA) broth [distilled water, 1 liter; peptone, 5.0 g; meat extract, 3.0 g; agar, 15.0 g (pH 7.2)] at 30°C. *Escherichia coli* DH5α was used for plasmid

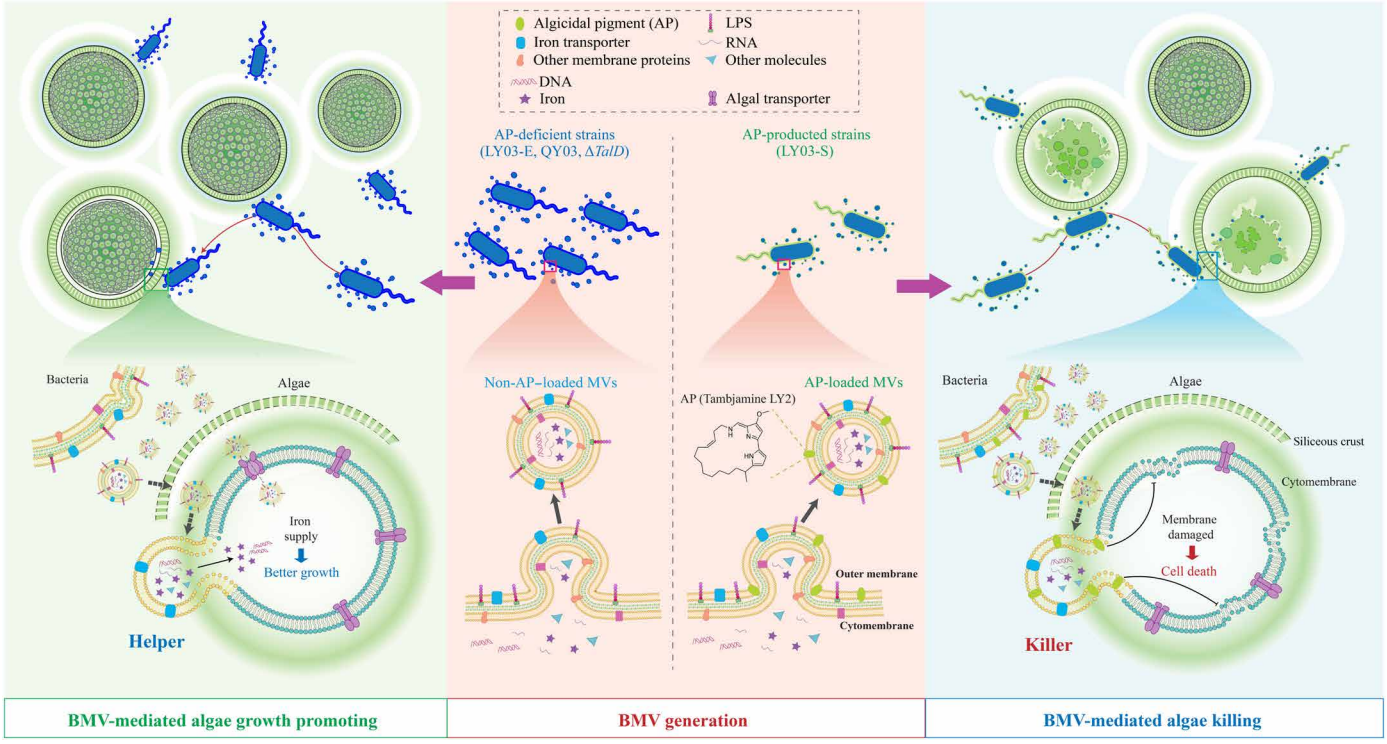

Fig. 7. A conceptual model of MV-mediated interkingdom interaction between LY03 and microalgae. LPS, lipopolysaccharide.

construction, and *E. coli* HB101 was used to introduce the plasmid into LY03 via conjugation. Genetic knockout in LY03 was conducted using pK18mobSacB. Antibiotics were added as necessary at final concentrations of kanamycin (50 μg/ml).

The algal strains used in this study are listed in table S3. These algal strains were provided by the College of Ocean and Earth Sciences, Xiamen University, Xiamen, China. The algal cultures were cultivated in f/2 medium (*39*) prepared with natural seawater at 20° ± 1°C under a 12-hour light/12-hour dark cycle with a light intensity of 50 μmol photons/m^2 per s.

Electron microscopic observation of algae and bacteria

LY03 cells were incubated in NA broth at 30°C with shaking at 150 rpm for 16 hours. Then, LY03 cells were collected by centrifugation at 3500*g* for 8 min and washed twice with phosphate-buffered saline (PBS). Then, the cells were fixed with 2.5% glutaraldehyde for 12 hours at 4°C. For SEM observation, the fixed cells were attached to a coverslip for 5 min, wiped dry, dehydrated in a graded ethanol series (30, 50, 70, 80, 95, and 100%), and then dried at the critical point. The dry cells were sputter-coated with gold on a copper mesh and imaged via SEM (JSM-6390LV, JEOL Co., Japan).

For TEM observation, LY03 and algal cells treated with MVs were fixed with glutaraldehyde solution (2.5%) overnight. After washing three times with PBS, the samples were gently embedded in 2% agar blocks. The resin block was cut into 70-nm ultrathin sections with a Leica Mltracut R microtome (Leica, Germany), double-stained with 2% uranyl acetate-lead citrate on a copper mesh, and then observed using TEM.

Cell growth assays, transcriptomic analysis, and whole-genome resequencing of LY03 and QY03

LY03 and QY03 were incubated in NA broth at 30°C with shaking at 150 rpm for 30 hours. The optical density (OD) of the bacterial cultures at 600 nm was measured every 2 hours to monitor cell growth. All treatments were performed in triplicate.

LY03 and QY03 were grown in NA medium to exponential phase (10 hours) and stationary phase (16 and 18 hours, respectively). Then, the bacterial cells were collected by centrifugation at 4°C. Total RNA was isolated using TRIzol reagent (Invitrogen, Carlsbad, CA, USA) according to the manufacturer's recommendations. For each of the samples, 10 μg of RNA was used for RNA sequencing library preparation by using the stranded Total RNA kit (Illumina TruSeq). After purification and enrichment, all libraries were sequenced using an Illumina HiSeq 2000 (Illumina, San Diego, CA, USA). All treatments were performed in triplicate. After calculation of the read counts of the transcripts, the expression difference of the transcript between samples was analyzed, and the differentially expressed genes among different groups were identified using EdgeR software (Majorbio, Shanghai, China).

To identify the mutation sites of QY03, the bacterial cells of QY03 were obtained according to the method described above for whole-genome resequencing. The genome of LY03 was used as the reference genome (*39*), and its gene clusters were predicted on the antiSMASH platform (https://antismash.secondarymetabolites.org/). After DNA extraction and sequencing of QY03, the adapters of sequencing reads were removed using fastp v0.20.0 and then mapped to the reference genome using the Burrows-Wheeler Aligner (BWA) software algorithm

mem (http://bio-bwa.sourceforge.net/). Then, the sequencing reads were filtered using Picard tools to remove PCR duplications. Sequencing depth and coverage relative to the reference genome were then calculated on the basis of the aligned BAM file. Genome Analysis Toolkit (GATK) software was used to locally realign reads near InDels to obtain a realigned BAM file, which eliminated false-positive single-nucleotide polymorphisms (SNPs) around InD. Snippy 4.6.0 software was then used to detect SNPs, small indels, etc. and to filter out loci with low sequencing depth and alignment quality values. Last, variant loci were annotated using snpEf to determine the impact of mutations on the genome (http://snpeff.sourceforge.net/SnpEff.html).

Construction of *TalD* mutant strain

The *TalD* mutant strain was constructed by the allelic exchange method. Two sets of primers listed in table S4 were designed to amplify the upstream and downstream regions of the target gene. Then, the two fragments were ligated by overlap PCR and subcloned and inserted into the pK18 suicide plasmid, which was introduced into *E. coli* DH5α (donor strain). After that, with the help of *E. coli* HB101 (helper strain), this recombination plasmid was transferred into LY03 (recipient strain) by triple parental conjugation. All the donor and helper strains were cultured in LB medium (*5*) [adding kanamycin (50 μg/ml)] at 37°C for 12 hours, and the recipient strain was cultured in NA medium at 30°C for 16 hours. These bacterial cells were washed and resuspended in 10 mM $MgSO_4$. Then, the donor strain, helper strain, and recipient strain were mixed at a ratio of 1:1:5 and incubated on NA agar plates at 30°C for 24 hours. To obtain the mutant, NA agar plates with kanamycin (50 μg/ml) and ampicillin (100 μg/ml) and NA agar plates with 5% sucrose were used to select transconjugants (first homologous recombination event) and mutants, respectively. The resulting colonies were purified and analyzed by colony PCR using primers LF/LR followed by DNA sequencing.

Construction of eGFP-labeled LY03

To obtain eGFP-LY03, the sequence of eGFP was amplified by PCR using primers from table S4 and cloned and inserted into the broad host expression plasmid pBBR1-Tac-MCS2. The recombination plasmids were then introduced into LY03 by triple parental conjugation. Last, NA agar plates with kanamycin (50 μg/ml) and ampicillin (100 μg/ml) were used to select strains and verified by colony PCR and sequencing.

MV isolation, purification, and characterization

To obtain MV solutions, bacterial cultures were collected at stationary phase followed by centrifugation at 10,000*g* for 30 min at 4°C, and supernatants were filtered through 0.45- and 0.22-μm vacuum filters to thoroughly remove the remaining bacterial cells. The filtrate was concentrated by ultrafiltration using a 100-kDa hollow fiber membrane (Millipore) and then ultracentrifuged at 150,000g at 4°C for 3 hours using a swing rotor (60 Ti, Beckman Coulter, USA) to obtain the crude MVs. The purified MVs were further obtained by density gradient centrifugation. The crude MVs were suspended in 1.3 ml of 45% OptiPrep solution (Sigma-Aldrich) with 10 mM Hepes-NaCl solution, transferred to ultracentrifuge tubes, and then overlaid with equal volumes of Optiprep at a series of concentrations (45, 40, 35, 30, 25, 20, 15, 10, and 0%). After centrifugation at 100,000g for 6 hours at 4°C in an SW 41Ti rotor, 1.3-ml fractions were collected from each gradient and recovered by diluting with at least five times volume of PBS buffer and pelleting in an ultracentrifuge (~150,000*g*, 1 hour, 4°C, SW41Ti rotor). The pellets were resuspended in PBS and stored at 4°C. The protein amount of purified MVs was determined using the Bradford protein assay according to the manufacturer's manual (Beyotime), and the protein concentration was used to indicate the MV concentration in the present study (*25*).

The size and concentration of purified MVs were characterized by Nano FCM. MV samples were diluted (1:10,000) and analyzed using the Flow Nano Analyzer (Nano FCM Inc., Xiamen, China) according to the manufacturer's instructions. The lasers were calibrated using 200-nm control beads, which were then regarded as a reference for particle concentration. In addition, a mixture of different-sized beads was analyzed to set a reference for size distribution. PBS was analyzed as a background signal. Particle concentration and size distribution were calculated using the nFCM software package, Nano FCM v. 2.0.

The morphology of purified MVs was captured using TEM. Ten microliters of MV solution was dropped onto a copper electron microscopy grid for 2 min and wiped dry, followed by negative staining with 1% uranyl acetate for 3 min and rinsed three times with PBS solution. Then, samples were dried at room temperature for 10 min and analyzed at 80 kV using Hitachi HT7800.

Extraction and identification of algicidal compounds

Treatments of MVs with proteinase K and nuclease

First, to rule out the possibility that the algicidal compounds carried by MVs are protein or nuclei acid, 1 U of ribonuclease A, 2 U of deoxyribonuclease I (DNase I), and proteinase K (100 μg/ml) were added to LY03-MVs and incubated at 37°C for 2 hours. These enzymes were removed by ultracentrifugation at 150,000*g* for 1.5 hours, and then the pellets were resuspended in PBS and applied to the determination of algicidal activity against alga *H. akashiwo*.

Sample collection for extraction and identification of algicidal compounds

LY03, QY03, and Δ*TalD* were grown in NA broth at 30°C for 24 hours. The total culture of LY03, QY03, and Δ*TalD* was extracted with equal volume of ethyl acetate. After the removal of solvents under vacuum, the extract was suspended in methanol (MeOH) for LC-MS analysis. For analyzing different culture components of LY03, the fermented LY03 broth was divided into four aliquots to prepare bacterial cells (LY03-Cells), cell-free supernatant (LY03-Sup.), supernatant after the removal of MVs [LY03-Sup. (no MVs)], and MVs from the supernatant (LY03-MVs), respectively. Then, each component was extracted and suspended as described above for LC-MS analysis. Another 6 liters of fermented LY03 broth was obtained for the extraction and analysis of algicidal compounds.

General experimental procedures in chemistry

Thin-layer chromatography on glass plates was coated with silica gel (200 to 300 mesh, Qingdao Marine Chemical Plant). Column chromatography was performed with silica gel (200 to 300 mesh, Qingdao Marine Chemical Plant), reversed-phase RP-18 (40 to 63 μm, Merck), and Sephadex LH-20 (Amersham Biosciences). Optical rotations were measured on AUTOPOL IV automatic polarimeter (RUDOLPH Inc.). Mass spectra for compound characterization were collected by Waters Acuity SQD LC-MS with the mode of electron spray ionization (ESI). High-resolution mass spectra were obtained by Thermo Fisher Scientific LTQ (linear ion trap quadrupole) Fourier transform

ion cyclotron resonance mass spectrometry (FTICR-MS). Compounds were purified by Waters Acuity SQD LC-MS with a Waters Nova-Pak C18 column (6 μm, 9.4 mm by 150 mm). NMR spectra were measured on a Bruker AVANCE (600 MHz) using tetramethylsilane as the internal standard, and chemical shift was reported in δ (parts per million), multiplicities (s = singlet, d = doublet, t = triplet, q = quartet, p = pentet, m = multiplet, and br = broad), and integration and coupling constants (*J* in Hz). ^{1}H and ^{13}C chemical shifts are relative to the solvent: δ_H 7.26 and δ_C 77.0 for $CDCl_3$; δ_H 2.50 and δ_C 39.5 for deuterated dimethyl sulfoxide; δ_H 2.05 and δ_C 29.8 and 206.2 for acetone-d_6. The structure elucidation, NMR and HRMS spectra, and details were shown in tables S5 and S6 and figs. S11 to S23. Structural assignments were made with additional information from gradient COSY, gradient HSQC, and gradient HMBC experiments.

LC-MS analysis

Sample analysis was performed using Waters Acuity SQD LC-MS with the mode of ESI. The injection volume was 20 μl. Samples were separated through a C18 column (4.6 mm by 100 mm with 1.7-μm particle size, Waters, Milford, MA, USA) with column temperature maintained at 40°C and mobile phases consisting of 0.1% trifluoroacetic acid in H_2O (mobile phase A) and MeOH (mobile phase B). The gradient started with 2 min of isocratic elution with 5% B (and 95% A), and B was increased to 100% in 2 to 20 min and kept for next 10 min. The flow rate for mobile phases was set at 1 ml/min.

Extraction of Tambjamine LY1 and Tambjamine LY2

Six liters of fermented LY03 broth was obtained, the ethanol extract of LY03 bacterial cells was fractionated by medium-pressure liquid chromatography over an RP-18 column (170 g) eluting with a MeOH-H_2O gradient (v/v, from 10 to 100% in 4 hours, flow rate of 25 ml/min) to afford fractions F1 to F6. The 100% MeOH fraction, F6, was sequentially subjected to Sephadex LH-20 (2.5 cm by 150 cm) eluting with MeOH to get two subfractions, the F6A and F6B. The F6A part was chromatographed using Waters Acuity SQD LC-MS with a Waters Nova-Pak C18 column (6 μm, 9.4 mm by 150 mm) under gradient elution in MEOH-H_2O (0 to 10 min, 5 to 100% MeOH, ultraviolet detection at 254 nm, flow rate of 20 ml/min). Tambjamine LY1 (9.5 mg) was isolated as a pure compound at a retention time of 7.5 min. Tambjamine LY2 (6.5 mg) was isolated from the F6B fraction at a retention time of 9.0 min by using the same elution method as used for Tambjamine LY1 purification.

Computational analysis

The specific rotation was calculated using ωB97X-D in conjunction with the 6-311+G(D,P) basis set (*62*). The calculated specific rotations ($|\alpha|_D$) of Tambjamine LY1 with proposed configurations of 20R and 20S are −82.69 and +82.69, respectively. Combined with the experimental value of −30.9, the absolute configuration of C-20 in Tambjamine LY1 is determined as R. Similarly, the calculated specific rotations ($|\alpha|_D$) of Tambjamine LY2 with proposed configurations of 20R and 20S are +100.02 and −100.02, respectively. Combined with the experimental value of +41.9, the absolute configuration of C-20 in Tambjamine LY2 is determined as R.

Protein and metabolite identification of MVs

To identify the protein component of MVs, purified MVs were collected from LY03 culture at the stationary phase. Then, 100 μg of MVs was mixed with 5× loading buffer, boiled for 5 min, and applied to 12% SDS–polyacrylamide gel electrophoresis. The resultant gels were cut into small (1 mm by 1 mm) pieces and were transferred into tubes, followed by rinse with PBS three times and trypsin digestion. Afterward, the obtained peptides were analyzed by the timsTOF Pro mass spectrometer (Bruker). The localization of identified proteins was predicted using the CELLO subcellular structure prediction software. In addition, Kyoto Encyclopedia of Genes and Genomes (KEGG) annotation was performed using eggNOG-mapper tool version 5.0.

LY03-S-MVs were also applied to metabolite detection. The metabolites of LY03-MVs were extracted using the cold MeOH method (*63*). Briefly, the MV samples were subjected to three rapid freeze-thaw cycles and then cooled (−20°C) for 1 hour. After that, the samples were vortexed and centrifuged for 15 min at 13,000 rpm at 4°C, and the supernatant was retained for vacuum evaporation. Metabolites were reconstituted in 100 μl of acetonitrile:water (1:1, v/v), and then the mixture was vortexed and centrifuged to remove insoluble material. Metabolite analysis was performed using the TripleTOF 5600+ (AB Sciex) system, LC-MS/MS parameters were controlled by Analyst 1.7.1 software, and the final data were obtained by Mutiquant 3.0.3 software.

Algicidal activity and spectrum determination of strains, MVs, and algicidal compounds

Bacterial cultures (LY03, QY03, and Δ*TalD*) and MVs were precultured, collected, and then added to 1 ml of tested algal cultures (table S3) at logarithmic phase. The growth of algal culture on 48-well plates was monitored by measuring chlorophyll autofluorescence at an excitation wavelength of 440 nm and an emission wavelength of 680 nm using a Tecan Spark plate reader. Algal cultures in NA medium or PBS were used as controls. The algicidal activity was calculated using the following equation

$$\text{Algicidal rates}\ (\%) = \frac{F0 - FT}{F0} \times 100$$

FT and *F*0 represent the fluorescence values of the algal cultures at different time points and at the beginning of the treatment period, respectively. All treatments were performed in triplicate.

To determine the algicidal activities of algicidal compounds, the growth of algae was monitored by counting the cell numbers using an automatic cell counter (Countstar IA1000, Shanghai Ruiyu Biotech Co. Ltd., Shanghai, China) since the presence of a maximum absorption peak at 425 nm for algicidal compounds may affect the results detected by the Tecan Spark plate reader. The algicidal rates were also calculated on the basis of the above formula.

Parameter settings of fluorescence microscopy

Confocal microscopy observation in this study was conducted on a Leica TCS SP8 system with a 100× oil objective. The fluorescence signals of DAPI and R18 were collected at 360 to 460 and 562 to 630 nm, respectively.

Zeiss Cell Discoverer 7 was used to track the interactions between algae and bacterial cells or their derived MVs. Images were acquired with the Zeiss Cell Discoverer 7 using a combination of three light-emitting diode modules with 488-, 555-, and 647-nm wavelengths. The following bandpass emission filters were used: 410 to 546, 555 to 645, and 645 to 700 nm. A Plan-Apochromat 50×/1.2 NA objective with a 2× tube lens was used for image acquisition. The Cell Discoverer chamber was set to 25°C, and then the mixed solutions of bacterial cells or MVs with algae were added to the 24-well plates and imaged continuously for 2 to 5 hours. Compiled

videos and images were processed using ZEISS ZEN software. Quantitative assessments of fluorescence in images were performed using FIJI software (National Institutes of Health).

Imaging of interactions of microalgae with eGFP-LY03 and LY03-MVs via fluorescence microscopy

The cellular membranes of *H. akashiwo* and *T. pseudonana* were stained with FM4-64 (10 μg/ml) for 2 to 6 hours at 25°C. eGFP-LY03 was cultivated to stationary phase, and then cells were collected and washed three times with PBS, followed by incubation with labeled microalgae. Purified LY03-MVs were fluorescently labeled with the lipophilic dye DiO (MVs-DiO) by incubation with algal cells for 1 hour at 37°C, according to the manufacturer's manual (Beyotime). The free dye was removed from the labeled MVs by washing twice with PBS (150,000*g*, 1.5 hours) and incubated with labeled microalgae, which were observed by Zeiss Cell Discoverer 7.

Chemotaxis assays of LY03 toward algae cells

Quantitative capillary chemotaxis assay

LY03 cells were inoculated in NA broth to stationary phase and then washed and resuspended at an OD_{600} of 0.04 in f/2 medium. Subsequently, cell suspensions were kept at 4°C for 24 hours to reduce motility. After that, an empty capillary (10 cm long with an internal diameter of 0.22 mm) was inserted into the Eppendorf tube containing the algal cultures, and the solution was siphoned by the capillary completely. Then, capillaries with f/2 medium only (control group) or algal cultures were heat-sealed on one end, and the capillary was inserted into a barrel of a disposable syringe prefilled with 300-μl cell suspension and sealed on one end. After incubation at 30°C for 2 hours, the capillaries were removed from the barrels and rinsed with f/2 medium, and 1 μl of the content was diluted 100 times. Last, 100 μl of the diluent was spread on NA plates. After incubation for 72 hours at 30°C, colonies were counted. All treatments were performed in triplicate.

Drop assay

LY03 cells were cultured in NA broth to stationary phase. Then, the cells were washed three times and resuspended in f/2 medium for drop assay. F/2 agar medium containing 0.18% Noble agar (Sigma-Aldrich, USA) was heated until the agar melted and then cooled to 40°C, and bacterial cells were added to the medium at a final $OD_{600} = 1$. After the plates solidified, 10 μl of f/2 medium (CK) or microalgal cells (*H. akashiwo* and *T. pseudonana*) in f/2 medium were dropped in the center of the plates and incubated at 30°C. Chemotactic responses of LY03 to microalgae were observed for 2 days. Every treatment had three replicates.

Determination of algal cellular membrane permeability

To determine the cell membrane permeability of *H. akashiwo*, algal cells were treated with MVs for 0, 60, and 180 min. Samples were collected by centrifugation and stained with PI (5 μg/ml; Beyotime) for 5 min in the dark at room temperature. Fluorescence was analyzed on a flow cytometer (Quanteon/ACEA, USA) using 535-nm excitation and a 617-nm bandpass filter for detection. For each sample, approximately 10,000 cells were analyzed. Three parallel samples were analyzed for each treatment.

The observation of membrane fusion between MVs and targeted microalgae

The fusion of MVs with the cytoplasmic membranes of targeted microalgae (*H. akashiwo*, *T. pseudonana*, and *P. tricornutum*) was monitored by octadecyl rhodamine B chloride (R18, TCI). One hundred micrograms of isolated MVs was labeled with R18 at a concentration of 80 μg/ml for 1 hour at room temperature. The unbound dye was removed by ultracentrifugation at 150,000*g*, and then the pellets were resuspended in PBS. Afterward, the algae were collected and washed three times with PBS. Thirty micrograms of labeled MVs was applied to the algal cells resuspended in PBS for 2 hours, and the fluorescence was observed by confocal microscopy (Leica TCS SP8 system).

Determination of MV-mediated interkingdom iron delivery

To test whether MVs were involved in iron delivery to microalgae, the incubation experiment of targeted microalgae (*H. akashiwo*, *T. pseudonana*, and *P. tricornutum*) with MVs was conducted. The MVs were collected from LY03 cultures at the exponential and stationary phase (LY03-E-MVs and LY03-S-MVs). The MVs were also collected to incubate with $FeCl_3$ solution (100 μM) to assess their capability of iron recruitment. Then iron-incubated LY03-E-MVs were added to the cultures of *H. akashiwo*, *T. pseudonana*, and *P. tricornutum*, when untreated and iron-incubated LY03-S-MVs were added to the cultures of *P. tricornutum*, at a final concentration of 30 μg/ml. The algal cultures were grown in f/2 medium without adding $FeCl_3$ (iron-deficient f/2 medium, f/2-Fe), using MVs as the sole iron source. The untreated MVs were also incubated with algal cultures to assess the MV effect on algal growth. In addition, to explore whether the iron is surface attached on or encapsulated inside the MVs, the iron-incubated MVs were further treated with 50, 10, and 1 μM EDTA when 50 μM EDTA has been verified to be able to chelate 100 μM iron in iron-incubated MV samples and then added to the algal cultures. The growth of microalgal cells was monitored by a Tecan Spark plate reader and an automatic cell counter. Simultaneously, microalgal cells cultured in f/2-Fe and in f/2-Fe medium with ferric iron addition at final concentration of 100 μM (f/2-Fe + i medium) were used as the respective negative and positive controls. All experiments were performed in triplicate.

To further determine whether siderophore was involved in iron acquisition of LY03 and its MVs, the occurrence of siderophore was assayed based on a chrome azurol S (CAS) method (*64*). Briefly, 20 μg of LY03 cells and LY03-MVs was collected at the exponential and stationary phase (LY03-S, LY03-E, LY03-E-MVs, and LY03-S-MVs) and suspended in 20 μl of PBS solution. The suspensions were then added to 20 μl of CAS assay solution (Coolaber, Beijing, China) in a 96-well plate. Simultaneously, 20 μl of PBS was also mixed with equal volumes of CAS assay solution as the negative control. After 0.5-hour incubation at room temperature, the color of solutions was observed.

Observation of MV-mediated DNA delivery

MVs were labeled with DAPI (10 μg/ml) for 1 hour at room temperature. The unbound dye was removed by ultracentrifugation at 150,000*g*, and then the pellets were resuspended in PBS. Afterward, external DNA was removed using 2 U of DNase I (Thermo Fisher Scientific, CA, USA) at 30°C for 30 min and washed again. Then, the labeled DAPI-MVs were incubated with *T. pseudonana* and *P. tricornutum* for 24 hours at 25°C, washed three times with PBS, and applied to monitor the fluorescence signals by confocal microscopy.

Detection of plasmid DNA and partial genomic DNA in MVs

The MVs of eGFP-LY03 cultured in NA were collected and incubated with 1 U of DNase I (Thermo Fisher Scientific) to digest DNA

attached to their surface. The reaction was performed in 300 μl at 37°C for 2 hours. To validate the digestion efficiency of DNase I, equal amounts of MVs were lysed (frozen and thawed five times followed by sonication for 30 s and then placed in ice for 30 s) before treated with DNase I. Simultaneously, the treatments of untreated and DNase-treated eGFP-pBBRMCS2 plasmid were also established. eGFP-LY03 was used as the positive control, and LY03 and LY03-MVs were used as the negative controls. Then, MV-related plasmid DNA was detected by PCR using the primers listed in table S3.

To detect MV-related partial genomic DNA, MVs of LY03 and Δ*TalD* were extracted and treated with DNase I as described above. Then, PCR experiments were conducted using the primers listed in table S4 to detect the presence of representative genomic genes, including 16*S* (phylogenetic biomarker), *OmpA* (outer membrane-related gene), *TalD* (key gene of pigment biosynthesis), and *betI* (potential regulatory gene of pigment biosynthesis).

Statistical analysis

All data are presented as the mean ± SEM from at least three independent experiments. Comparisons between two groups were performed by unpaired *t* test. Statistical analyses were performed with GraphPad Prism software 9.0, and a statistical significance level of less than 0.05 was accepted.

Supplementary Materials

This PDF file includes:

Supplementary Text
Figs. S1 to S23
Tables S1 to S6
Legends for movies S1 to S5
References

Other Supplementary Material for this manuscript includes the following:

Movies S1 to S5

REFERENCES AND NOTES

1. C. Schwechheimer, M. J. Kuehn, Outer-membrane vesicles from Gram-negative bacteria: Biogenesis and functions. *Nat. Rev. Microbiol.* **13**, 605–619 (2015).
2. M. Toyofuku, N. Nomura, L. Eberl, Types and origins of bacterial membrane vesicles. *Nat. Rev. Microbiol.* **17**, 13–24 (2019).
3. J. Rivera, R. J. B. Cordero, A. S. Nakouzi, S. Frases, A. Nicola, A. Casadevall, *Bacillus anthracis* produces membrane-derived vesicles containing biologically active toxins. *Proc. Natl. Acad. Sci. U.S.A.* **107**, 19002–19007 (2010).
4. S. J. Biller, F. Schubotz, S. E. Roggensack, A. W. Thompson, R. E. Summons, S. W. Chisholm, Bacterial vesicles in marine ecosystems. *Science* **343**, 183–186 (2014).
5. C. Li, L. Zhu, D. Wang, Z. Wei, X. Hao, Z. Wang, T. Li, L. Zhang, Z. Lu, M. Long, Y. Wang, G. Wei, X. Shen, T6SS secretes an LPS-binding effector to recruit OMVs for exploitative competition and horizontal gene transfer. *ISME J.* **16**, 500–510 (2022).
6. A. J. McBroom, M. J. Kuehn, Release of outer membrane vesicles by Gram-negative bacteria is a novel envelope stress response. *Mol. Microbiol.* **63**, 545–558 (2007).
7. S. Erdmann, B. Tschitschko, L. Zhong, M. J. Raftery, R. Cavicchioli, A plasmid from an Antarctic haloarchaeon uses specialized membrane vesicles to disseminate and infect plasmid-free cells. *Nat. Microbiol.* **2**, 1446–1455 (2017).
8. V. Tiku, M. W. Tan, Host immunity and cellular responses to bacterial outer membrane vesicles. *Trends Immunol.* **42**, 1024–1036 (2021).
9. D. Schatz, S. Rosenwasser, S. Malitsky, S. G. Wolf, E. Feldmesser, A. Vardi, Communication via extracellular vesicles enhances viral infection of a cosmopolitan alga. *Nat. Microbiol.* **2**, 1485–1492 (2017).
10. L. M. Mashburn, M. Whiteley, Membrane vesicles traffic signals and facilitate group activities in a prokaryote. *Nature* **437**, 422–425 (2005).
11. M. Toyofuku, K. Morinaga, Y. Hashimoto, J. Uhl, H. Shimamura, H. Inaba, P. Schmitt-Kopplin, L. Eberl, N. Nomura, Membrane vesicle-mediated bacterial communication. *ISME J.* **11**, 1504–1509 (2017).
12. A. Guerrero-Mandujano, C. Hernández-Cortez, J. A. Ibarra, G. Castro-Escarpulli, The outer membrane vesicles: Secretion system type zero. *Traffic* **18**, 425–432 (2017).
13. J. L. Baker, L. Chen, J. A. Rosenthal, D. Putnam, M. P. DeLisa, Microbial biosynthesis of designer outer membrane vesicles. *Curr. Opin. Biotechnol.* **29**, 76–84 (2014).
14. N. Krishnan, L. J. Kubiatowicz, M. Holay, J. Zhou, R. H. Fang, L. Zhang, Bacterial membrane vesicles for vaccine applications. *Adv. Drug Deliv. Rev.* **185**, 114294 (2022).
15. I. K. Herrmann, M. J. A. Wood, G. Fuhrmann, Extracellular vesicles as a next-generation drug delivery platform. *Nat. Nanotechnol.* **16**, 748–759 (2021).
16. A. Chronopoulos, R. Kalluri, Emerging role of bacterial extracellular vesicles in cancer. *Oncogene* **39**, 6951–6960 (2020).
17. Y. J. Yu, X. H. Wang, G. C. Fan, Versatile effects of bacterium-released membrane vesicles on mammalian cells and infectious/inflammatory diseases. *Acta Pharmacol. Sin.* **39**, 514–533 (2018).
18. L. Katsir, O. Bahar, Bacterial outer membrane vesicles at the plant–pathogen interface. *PLOS Pathog.* **13**, e1006306 (2017).
19. H. Gao, Y. Jiang, L. Wang, G. Wang, W. Hu, L. Dong, S. Wang, Outer membrane vesicles from a mosquito commensal mediate targeted killing of Plasmodium parasites via the phosphatidylcholine scavenging pathway. *Nat. Commun.* **14**, 5157 (2023).
20. Y. Liu, Q. Liu, L. Zhao, S. W. Dickey, H. Wang, R. Xu, T. Chen, Y. Jian, X. Wang, H. Lv, M. Otto, M. Li, Essential role of membrane vesicles for biological activity of the bacteriocin micrococcin P1. *J. Extracell. Vesicles* **11**, e12212 (2022).
21. M. Wang, Y. Nie, X.-L. Wu, Membrane vesicles from a Dietzia bacterium containing multiple cargoes and their roles in iron delivery. *Environ. Microbiol.* **23**, 1009–1019 (2021).
22. M. Toyofuku, S. Schild, M. Kaparakis-Liaskos, L. Eberl, Composition and functions of bacterial membrane vesicles. *Nat. Rev. Microbiol.* **21**, 415–430 (2023).
23. X. Wang, W. J. Eagen, J. C. Lee, Orchestration of human macrophage NLRP3 inflammasome activation by Staphylococcus aureus extracellular vesicles. *Proc. Natl. Acad. Sci. U.S.A.* **117**, 3174–3184 (2020).
24. J. Jäger, S. Keese, M. Roessle, M. Steinert, A. B. Schromm, Fusion of Legionella pneumophila outer membrane vesicles with eukaryotic membrane systems is a mechanism to deliver pathogen factors to host cell membranes. *Cell. Microbiol.* **17**, 607–620 (2015).
25. T. M. Tran, C. P. Chng, X. Pu, Z. Ma, X. Han, X. Liu, L. Yang, C. Huang, Y. Miao, Potentiation of plant defense by bacterial outer membrane vesicles is mediated by membrane nanodomains. *Plant Cell* **34**, 395–417 (2022).
26. J. R. Seymour, S. A. Amin, J. B. Raina, R. Stocker, Zooming in on the phycosphere: The ecological interface for phytoplankton–bacteria relationships. *Nat. Microbiol.* **2**, 17065 (2017).
27. J. A. Hilton, R. A. Foster, H. James Tripp, B. J. Carter, J. P. Zehr, T. A. Villareal, Genomic deletions disrupt nitrogen metabolism pathways of a cyanobacterial diatom symbiont. *Nat. Commun.* **4**, 1767 (2013).
28. M. T. Croft, A. D. Lawrence, E. Raux-Deery, M. J. Warren, A. G. Smith, Algae acquire vitamin B_{12} through a symbiotic relationship with bacteria. *Nature* **438**, 90–93 (2005).
29. E. Kazamia, R. Sutak, J. Paz-Yepes, R. G. Dorrell, F. R. J. Vieira, J. Mach, J. Morrissey, S. Leon, F. Lam, E. Pelletier, J. M. Camadro, C. Bowler, E. Lesuisse, Endocytosis-mediated siderophore uptake as a strategy for Fe acquisition in diatoms. *Sci. Adv.* **4**, eaar4536 (2018).
30. H. Peng, L. E. de-Bashan, Y. Bashan, B. T. Higgins, Indole-3-acetic acid from *Azosprillum brasilense* promotes growth in green algae at the expense of energy storage products. *Algal. Res.* **47**, 101845 (2020).
31. S. Nair, Z. Zhang, H. Li, H. Zhao, H. Shen, S.-J. Kao, N. Jiao, Y. Zhang, Inherent tendency of *Synechococcus* and heterotrophic bacteria for mutualism on long-term coexistence despite environmental interference. *Sci. Adv.* **8**, eabf4792 (2022).
32. C. Brownlee, K. E. Helliwell, Y. Meeda, D. McLachlan, E. A. Murphy, G. L. Wheeler, Regulation and integration of membrane transport in marine diatoms. *Semin. Cell Dev. Biol.* **134**, 79–89 (2023).
33. A. Kouzuma, K. Watanabe, Exploring the potential of algae/bacteria interactions. *Curr. Opin. Biotechnol.* **33**, 125–129 (2015).
34. F. Stock, G. Bilcke, S. De Decker, C. M. Osuna-Cruz, K. Van den Berge, E. Vancaester, L. De Veylder, K. Vandepoele, S. Mangelinckx, W. Vyverman, Distinctive growth and transcriptional changes of the diatom *Seminavis robusta* in response to quorum sensing related compounds. *Front. Microbiol.* **11**, 1240 (2020).
35. E. L. Harvey, R. W. Deering, D. C. Rowley, A. El Gamal, M. Schorn, B. S. Moore, M. D. Johnson, T. J. Mincer, K. E. Whalen, A bacterial quorum-sensing precursor induces mortality in the marine Coccolithophore, *Emiliania huxleyi*. *Front. Microbiol.* **7**, 59 (2016).
36. Y. Li, H. Zhu, X. Lei, H. Zhang, C. Guan, Z. Chen, W. Zheng, H. Xu, Y. Tian, Z. Yu, T. Zheng, The first evidence of deinoxanthin from *Deinococcus* sp. Y35 with strong algicidal effect on the toxic dinoflagellate *Alexandrium tamarense*. *J. Hazard. Mater.* **290**, 87–95 (2015).
37. S. Zhang, W. Zheng, H. Wang, Physiological response and morphological changes of *Heterosigma akashiwo* to an algicidal compound prodigiosin. *J. Hazard. Mater.* **385**, 121530 (2020).
38. Z. Zhang, D. Li, R. Xie, R. Guo, S. Nair, H. Han, G. Zhang, Q. Zhao, L. Zhang, N. Jiao, Y. Zhang, Plastoquinone synthesis inhibition by tetrabromo biphenyldiol as a widespread algicidal mechanism of marine bacteria. *ISME J.* **17**, 1979–1992 (2023).

39. Y. Li, H. Zhu, Q. Lai, X. Lei, Z. Chen, H. Zhang, Y. Tian, W. Zheng, T. Zheng, *Chitinimonas prasina* sp. nov., isolated from lake water. *Int. J. Syst. Evol. Microbiol.* **64**, 3005–3009 (2014).
40. Y. Li, X. Lei, H. Zhu, H. Zhang, C. Guan, Z. Chen, W. Zheng, L. Fu, T. Zheng, Chitinase producing bacteria with direct algicidal activity on marine diatoms. *Sci. Rep.* **6**, 21984 (2016).
41. P. Li, S. He, X. Zhang, Q. Gao, Y. Liu, L. Liu, Structures, biosynthesis, and bioactivities of prodiginine natural products. *Appl. Microbiol. Biotechnol.* **106**, 7721–7735 (2022).
42. K. J. Picott, J. A. Deichert, E. M. deKemp, G. Schatte, F. Sauriol, A. C. Ross, Isolation and characterization of tambjamine MYP1, a macrocyclic tambjamine analogue from marine bacterium *Pseudoalteromonas citrea*. *Medchemcomm.* **10**, 478–483 (2019).
43. M. Wang, Y. Nie, X. L. Wu, Extracellular heme recycling and sharing across species by novel mycomembrane vesicles of a Gram-positive bacterium. *ISME J.* **15**, 605–617 (2021).
44. S. Gill, R. Catchpole, P. Forterre, Extracellular membrane vesicles in the three domains of life and beyond. *FEMS Microbiol. Rev.* **43**, 273–303 (2019).
45. M. G. Sartorio, E. J. Pardue, M. F. Feldman, M. F. Haurat, Bacterial outer membrane vesicles: From discovery to applications. *Annu. Rev. Microbiol.* **75**, 609–630 (2021).
46. K. J. Coyne, Y. Wang, G. Johnson, Algicidal bacteria: A review of current knowledge and applications to control harmful algal blooms. *Front. Microbiol.* **13**, 871177 (2022).
47. N. Meyer, A. Bigalke, A. Kaulfuß, G. Pohnert, Strategies and ecological roles of algicidal bacteria. *FEMS Microbiol. Rev.* **41**, 880–899 (2017).
48. J. Shi, W. Wang, F. Wang, S. Lei, S. Shao, C. Wang, G. Li, T. An, Efficient inactivation of harmful algae K. mikimotoi by a novel algicidal bacterium via a rare direct contact pathway: Performances and mechanisms. *Sci. Total Environ.* **892**, 164401 (2023).
49. S. Brameyer, L. Plener, A. Müller, A. Klingl, G. Wanner, K. Jung, Outer membrane vesicles facilitate trafficking of the hydrophobic signaling molecule CAI-1 between *Vibrio harveyi* cells. *J. Bacteriol.* **200**, e00740–e00717 (2018).
50. J. M. Bomberger, D. P. MacEachran, B. A. Coutermarsh, S. Ye, G. A. O'Toole, B. A. Stanton, Long-distance delivery of bacterial virulence factors by *Pseudomonas aeruginosa* outer membrane vesicles. *PLOS Pathog.* **5**, e1000382 (2009).
51. V. Gujrati, S. Kim, S. H. Kim, J. J. Min, H. E. Choy, S. C. Kim, S. Jon, Bioengineered bacterial outer membrane vesicles as cell-specific drug-delivery vehicles for cancer therapy. *ACS Nano* **8**, 1525–1537 (2014).
52. Y. Liu, S. Alexeeva, K. A. Y. Defourny, E. J. Smid, T. Abee, Tiny but mighty: Bacterial membrane vesicles in food biotechnological applications. *Curr. Opin. Biotechnol.* **49**, 179–184 (2018).
53. J. C. Caruana, S. A. Walper, Bacterial membrane vesicles as mediators of microbe – Microbe and microbe – Host community interactions. *Front. Microbiol.* **11**, 432 (2020).
54. J. Lin, W. Zhang, J. Cheng, X. Yang, K. Zhu, Y. Wang, G. Wei, P. Y. Qian, Z. Q. Luo, X. Shen, A *Pseudomonas* T6SS effector recruits PQS-containing outer membrane vesicles for iron acquisition. *Nat. Commun.* **8**, 14888 (2017).
55. J. Morrissey, C. Bowler, Iron utilization in marine cyanobacteria and eukaryotic algae. *Front. Microbiol.* **3**, 43 (2012).
56. S. A. Amin, D. H. Green, M. C. Hart, F. C. Küpper, W. G. Sunda, C. J. Carrano, Photolysis of iron–siderophore chelates promotes bacterial–algal mutualism. *Proc. Natl. Acad. Sci. U.S.A.* **106**, 17071–17076 (2009).
57. D. K. Yadav, A. Singh, V. Agrawal, N. Yadav, "Algal biomass" in *Bioprospecting of Plant Biodiversity for Industrial Molecules*, S. K. Upadhyay, S. P. Singh, Eds. (Wiley, 2021), pp. 303–334.
58. E. T. Yu, F. J. Zendejas, P. D. Lane, S. Gaucher, B. A. Simmons, T. W. Lane, Triacylglycerol accumulation and profiling in the model diatoms *Thalassiosira pseudonana* and *Phaeodactylum tricornutum* (Baccilariophyceae) during starvation. *J. Appl. Phycol.* **21**, 669–681 (2009).
59. P. G. Kroth, A. M. Bones, F. Daboussi, M. I. Ferrante, M. Jaubert, M. Kolot, M. Nymark, C. R. Bártulos, A. Ritter, M. T. Russo, M. Serif, P. Winge, A. Falciatore, Genome editing in diatoms: Achievements and goals. *Plant Cell Rep.* **37**, 1401–1408 (2018).
60. E. J. O'Donoghue, A. M. Krachler, Mechanisms of outer membrane vesicle entry into host cells. *Cell. Microbiol.* **18**, 1508–1517 (2016).
61. L. Xiu, Y. Wu, G. Lin, Y. Zhang, L. Huang, Bacterial membrane vesicles: Orchestrators of interkingdom interactions in microbial communities for environmental adaptation and pathogenic dynamics. *Front. Immunol.* **15**, 1371317 (2024).
62. A. D. Mclean, G. S. Chandler, Contracted gaussian-basis sets for molecular calculations. I. Second row atoms, Z=11-18. *J. Chem. Phys.* **72**, 5639–5648 (1980).
63. M. Sun, L. Li, Y. Niu, Y. Wang, Q. Yan, F. Xie, Y. Qiao, J. Song, H. Sun, Z. Li, S. Lai, H. Chang, H. Zhang, J. Wang, C. Yang, H. Zhao, J. Tan, Y. Li, S. Liu, B. Lu, M. Liu, G. Kong, Y. Zhao, C. Zhang, S.-H. Lin, C. Luo, S. Zhang, C. Shan, PRMT6 promotes tumorigenicity and cisplatin response of lung cancer through triggering 6PGD/ENO1 mediated cell metabolism. *Acta Pharm. Sin. B.* **13**, 157–173 (2023).
64. B. Schwyn, J. B. Neilands, Universal chemical assay for the detection and determination of siderophores. *Anal. Biochem.* **160**, 47–56 (1987).
65. Y. Li, J. Liang, S. Yang, J. Yao, K. Chen, L. Yang, W. Zheng, Y. Tian, Finding novel chemoreceptors that specifically sense and trigger chemotaxis toward polycyclic aromatic hydrocarbons in *Novosphingobium pentaromativorans* US6-1. *J. Hazard. Mater.* **416**, 126246 (2021).
66. Y. Kinoshita, H. Niwa, E. Uchida-Fujii, T. Nukada, Establishment and assessment of an amplicon sequencing method targeting the 16S-ITS-23S rRNA operon for analysis of the equine gut microbiome. *Sci. Rep.* **11**, 11884 (2021).

Acknowledgments: We are grateful to L. Yao, C. Wu, Q. Liu, L. Huang, and X. Sun from the Analysis and Measurement Center, School of Life Sciences, Xiamen University for help in performing of TEM, SEM, Zeiss Cell Discoverer 7, Leica TCS SP8, and Nano FCM, respectively. **Funding:** This work was supported by grants from the National Key R&D Program and the National Natural Science Foundation of China (nos. 41976141 and 42376144 to Y.T. and nos. 2022YFC2804100, 22025702, 82021003, 82151211, and 92253303 to X.D.), Natural Science Foundation of Fujian Province (no. 2023 J02002), the Project "111" sponsored by the State Bureau of Foreign Experts and Ministry of Education of China (#BP2018017), and the New Cornerstone Science Foundation through the XPLORER PRIZE to X.D. **Author contributions:** Y.T., X.D., and Y.L. outset and designed experiments; Y.L., Y.W., S.S., M.Y., Y.G., and J.W. performed experiments; Y.L., Y.W., X.L., and A.W. analyzed the data. Y.T., X.D., X.L., Y.W., and Y.L. wrote the paper. Y.T. and X.D. received projects and contributed reagents and materials. All authors importantly discussed and revised the manuscript. All authors commented on the manuscript before submission. All authors read and approved the final manuscript. **Competing interests:** The authors declare that they have no competing interests. **Data and materials availability:** All data needed to evaluate the conclusions in the paper are present in the paper and/or the Supplementary Materials. The raw sequence data (including transcriptomes and resequencing of QY03 under experiment ID OEX025297 and OEX025298) that support the findings of this study have been deposited in the NODE repository (www.biosino.org/node/index) under project ID OEP004642. The genome of LY03 and the assembly of QY03 have been deposited in eLMSG (www.biosino.org/elmsg/index) with the accession numbers LMSG_G000026929.1 and LMSG_G000026930.1.

Submitted 12 December 2023
Accepted 28 June 2024
Published 7 August 2024
10.1126/sciadv.adn4526